A Hierarchic 3D Finite Element for Laminated Composites

Guido Kuhlmann and Raimund Rolfes
Airbus Germany, Stress Department, Hamburg, Germany
German Aerospace Centre, Institute of Structural Mechanics, Braunschweig, Germany

ABSTRACT: In this paper a new 3D multilayer element is presented for analysis of thick-walled laminated composites. This element uses two steps to calculate the full stress tensor. In the first step the in-plane stresses are computed from the material law using a displacement approximation, and then the transverse stresses are calculated from the 3D equilibrium equations. Since the 3D equilibrium equations require high-order interpolation functions, a hierarchic interpolation of displacements is used. The new element is compared with existing ones, e.g. from MSC.MARC.

1 Introduction

The Finite-Element-Method is the most common method for stress analysis used by industry. Analysing composites is usually carried out by means of plate and shell elements, which are based on plate and shell theories. These theories approximate the distribution of the displacement through the thickness of the laminate by a known function. The most simple plate theory is the classical plate theory (CPT), a straightforward extension of Kirchhoff's plate theory (1850) [14]. The CPT assumes, that no transverse shear strains occur through the thickness of the plate. This is a very restrictive assumption for the analysis of laminated composites since they usually have very low out-of-plane shear stiffness. Additionally, Kirchhoff's assumption results in $C^{(1)}$-continuity requirements for the out-of-plane displacements. For this reason Whitney and Pagano [32] developed, based on Reissner-Mindlin's first-order shear deformation theory (FSDT) [15, 24], a bending theory for anisotropic laminated plates in order to relax the restrictions of the CPT. In this refined theory the transverse shear strains are assumed to be constant and a shear correction factor is used to compute the shear strain energy accurately. However, with just one shear correction factor it is impossible to approximate the different distributions of transverse shear stresses in laminated composites. In addition, the shear correction factor depends on the properties of the laminate and hence it is not applicable in general. For this reason Rohwer [25, 26] proposed to supplement the FSDT by improved transverse shear stiffnesses. These are calculated using an equilibrium approach as well as the assumption of two cylindrical bending modes. By means of the improved stiffnesses, the FSDT provides very good displacement results. However, due to the assumption of layerwise constant transverse shear strains, it leads to constant transverse shear stresses when calculated from the material law. Post-processing methods can be used to obtain improved transverse shear as well as transverse normal stresses through integration of the 3D equilibrium equations [17, 22]. However, the calculation of transverse stresses using the equilibrium equations requires computation of higher order derivatives. At least quadratic ones are needed to obtain transverse shear stresses and cubic ones to obtain the transverse normal stress. Based on this approach Rolfes and Rohwer [27, 28] proposed an extended 2D-

method for calculating transverse stresses in laminated composites. In this refined method the full stress tensor can be computed by quadratic displacement approximations only. Two essential advantages appear using this improved method. The main advantage is the satisfaction of all continuity conditions on displacements as well as on transverse stresses at interfaces and boundaries. Furthermore this equilibrium method uses the improved transverse stiffnesses by which computation of stresses can be done without shear correction factors. This extended 2D-method has been implemented into the software package TRAVEST to be used as a postprocessor for results from two-dimensional computations with MSC.NASTRAN. Higher order theories have also been proposed in order to compute mainly improved transverse stresses. Excellent reviews of these theories are presented by Noor [17], Rohwer [26] or Reddy [23].

While thin structures are analysed by shell elements mainly based on FSDT, thick structures must be calculated using 3D elements. The use of homogeneous, anisotropic 3D elements to analyse composite structures becomes inefficient, since an adequate accuracy requires between three and five elements along the thickness of each layer [4]. 3D multilayer elements, which are offered by some commercial FE-Codes, are not fully developed. Such elements are based, for example, on quadratic approximations of in-plane displacements u and v and out-of-plane displacements w [12, 16]. However, these assumptions are insufficient to analyse thick structures, since the in-plane displacements of thick structures show strong zig-zag distributions in thickness direction [19]. Hence the calculated transverse stresses are not accurate. In addition, not only the displacements but also their derivatives with respect to the thickness coordinate are assumed continuous. This implies that the transverse shear strains are continuous across the material interfaces and by using the material law, the transverse stresses are discontinuous. Thus, equilibrium at the interfaces is violated. The 3D equilibrium equations can also be used for 3D elements to obtain a refinement of transverse stresses. However, the assumptions, which in [27, 28] led to the extended 2D-method based on quadratic displacement functions, are not valid for thick composites. Therefore, using 3D equilibrium equations for thick composites require computation of higher order derivatives and thus high-order shape functions have to be used for such elements.

Besides the 2D- and 3D-standard formulations mentioned above hierarchical methods are proposed for calculating composite structures. A general consideration of hierarchical 2D- and 3D finite elements can be found in [31], [34] or [30]. An extension of the hierarchical method to a method for computing laminated composites was e.g. given by Babuška et al. [2] or Actis et al. [1]. However using hierarchical methods combined with the material law to calculate the full stress tensor requires high polynomial orders.

Therefore, in this paper a new 3D multilayer element is presented for analysis of thick laminated composites. This element uses two steps to calculate the full stress tensor. In the first step the in-plane stresses are computed from the material law using a displacement approximation and then in the second step transverse stresses are calculated from the 3D equilibrium equations. As mentioned before the 3D equilibrium equations require high-order interpolation functions. Therefore a hierarchical interpolation of displacements is used. The hierarchical shape functions are built from Legendre polynomials, which are orthogonal. The use of orthogonal polynomials brings some numerical advantages, like avoidance of round-off errors usually associated with polynomials of high degree. In addition, coupling between hierarchical degrees of freedom is minimized and a more dominant diagonal form of the stiffness matrix is obtained. This has important consequences of ensuring an improved condition of the stiffness matrix. By using this element within a p-method a faster rate convergence during the iteration process is achieved as compared to non-hierarchical functions.

2 Standard and hierarchical finite element concepts

The hierarchical concept for finite element shape functions has been investigated during the past 20 years [3, 7, 30, 31, 33]. While in the standard *h*-version of the finite element method the mesh is refined to achieve convergence the polynomial degree of the shape functions remains unchanged. Hence usually low order approximations of degree *p*=1 or *p*=2 are used. In the *p*-version the mesh keeps unchanged and the polynomial degree of the shape functions is increased. A certain disadvantage emerges by using standard nodal shape functions. Since by increasing the polynomial order for standard elements new shape functions must be built and all preceded calculations must be repeated. If the refinement is made hierarchically then an increase of the polynomial degree does not alter the lower order shape functions (see Figure 1). So the stiffness matrix of a preceded step is preserved and the solution with the lower polynomial order can be used to start the next computation step.

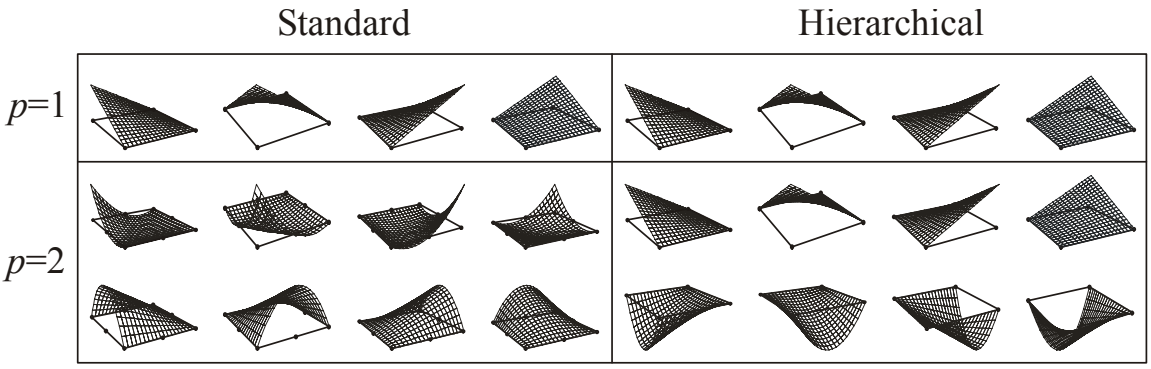

Figure 1: Set of standard and hierarchical shape functions

As mentioned above the hierarchical concept leads to a stiffness matrix with a dominant diagonal. In [33] it was shown, that the condition number of the stiffness matrix is improved by an order of magnitude if hierarchical shape functions are applied.

2.1 Standard shape functions for hexahedral elements

Standard shape functions are the basis for most finite element formulations. These shape functions satisfy the usual properties that $N_i = 1$ at node i and $N_i = 0$ at all other nodes. With the natural coordinates $\xi, \eta, \zeta \in [-1,1]$ we have:

Linear element (8 nodes):

$$N_i = \tfrac{1}{8}(1+\xi_0)(1+\eta_0)(1+\zeta_0) \tag{1}$$

Quadratic element (20 nodes):

Corner nodes (8 nodes):

$$N_i = \tfrac{1}{8}(1+\xi_0)(1+\eta_0)(1+\zeta_0)(\xi_0+\eta_0+\zeta_0-2) \tag{2}$$

Typical mid-side node (12 nodes):

$$\begin{aligned} &\xi_i = 0 \quad \eta_i = \pm 1 \quad \zeta_i = \pm 1 \\ &N_i = \tfrac{1}{4}(1+\xi^2)(1+\eta_0)(1+\zeta_0) \end{aligned} \tag{3}$$

with

$$\xi_0 = \xi\xi_i \quad \eta_0 = \eta\eta_i \quad \zeta_0 = \zeta\zeta_i \tag{4}$$

in which ξ_i, η_i and ζ_i are the natural coordinates at node i.

2.2 Hierarchical shape functions for hexahedral elements

The first 8 shape functions are the 8 functions for the linear element. But then in contrast to the standard shape functions all other hierarchical shape functions satisfy only the condition to be zero at the 8 corner nodes. In the hierarchical concept there are two different types of spaces, which are used for the 3D composite element: the isotropic space $\mathscr{S}^p$ and the anisotropic space $\mathscr{S}^{p,p,q}$. The polynomial degree for the isotropic space is the same in all local directions, whereas the polynomial degree for the anisotropic space can be varied in local directions. In the anisotropic space all shape functions in ξ-and η-direction are associated with the polynomial degree p. The value q defines the degree of all shape functions in ζ-direction (see Figure 2).

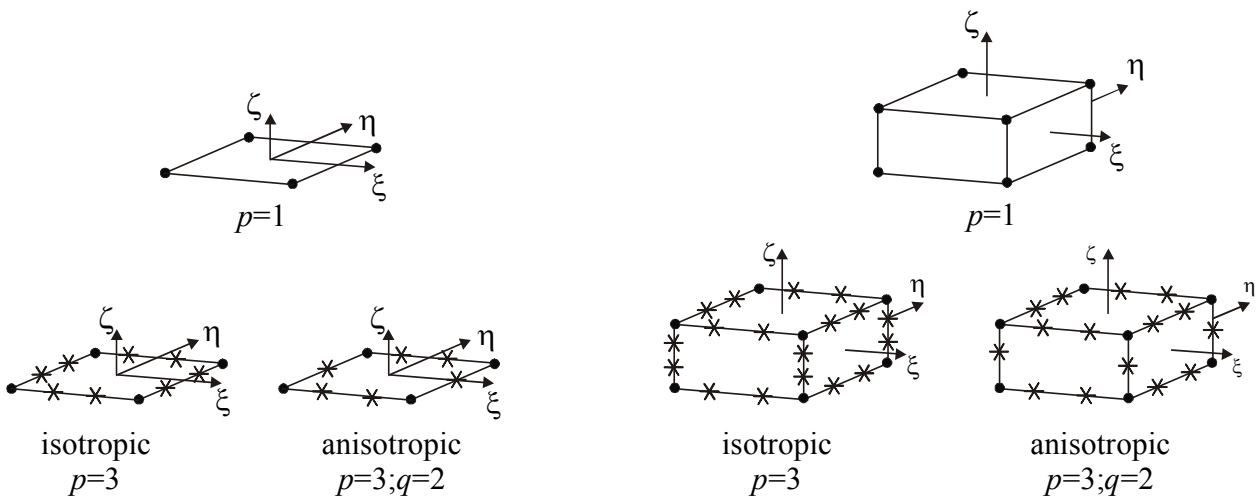

Figure 2: Isotropic and anisotropic spaces in 2D and 3D

For defining hierarchical basis functions there is no optimal function set, but there are two important conditions [29]:

1. The element stiffness matrices should have a condition number as small as possible in order to minimize round-off errors, which usually occur when increasing p.
2. The computation of element stiffness matrices and load vectors should be as efficient as possible.

These two considerations lead to element basis functions constructed from simple polynomial functions with certain orthogonality properties, e.g. Legendre or Chebyshev polynomials. Additionally, the basis functions should be hierarchic, i.e the basis functions of degree p should be embedded in the set of basis functions of degree p+1. In the 3D composite element formulation the normalized integral of the Legendre polynomials is used [30]:

$$\phi_n(x) = \sqrt{\frac{2n-1}{2}} \int_{-1}^{x} P_{n-1}(t)\, dt = \frac{1}{\sqrt{4n-2}} \left(P_n(x) - P_{n-2}(x) \right) \quad n \geq 2\,, \tag{5}$$

where $P_n(x)$ are Legendre polynomials. The first five Legendre polynomials are:

$$\begin{aligned} P_0(x) &= 1 \\ P_1(x) &= x \\ P_2(x) &= \tfrac{1}{2}\left(3x^2 - 1\right) \\ P_3(x) &= \tfrac{1}{2}\left(5x^3 - 3x\right) \\ P_4(x) &= \tfrac{1}{8}\left(35x^4 - 30x^2 + 3\right) \end{aligned} \tag{6}$$

Additional Legendre polynomials can be generated using Bonnet's recursion formula:

$$(n+1) P_{n+1}(x) = (2n+1)\, x P_n(x) - n P_{n-1}(x)\,. \tag{7}$$

It is seen from equation (6) that Legendre polynomials take the values ±1 at $x = \pm 1$. Thus they cannot qualify as hierarchical shape functions if nodes are located at $x = \pm 1$, since hierarchical shape functions must vanish at node points. That's why equation (5) is used to construct hierarchical shape functions.

The implementation of the p-version for the three dimensional composite finite element uses basis functions introduced by Szabó and Babuška [30], which are based on the Legrendre polynomials in equation (5). Since the three-dimensional shape functions for hexahedral elements (see Figure 3) correspond to nodes, edges, faces and bodies they can be classified into four groups:

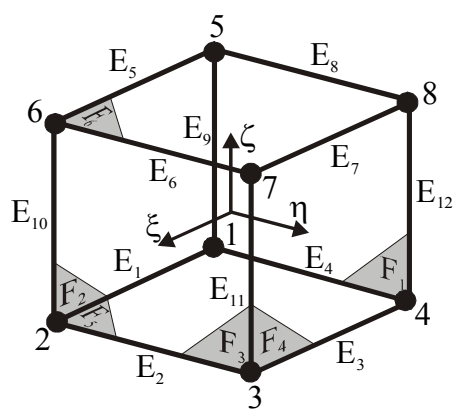

Figure 3: The standard hexahedral element

Isotropic Space $\mathscr{S}^p$

Nodal shape functions (Nodal modes)

There are eight nodal shape functions. These are the same as the shape functions used in eight-noded hexahedral elements in *h*-version concepts.

$$\begin{aligned} N_1(\xi,\eta,\zeta) &= \tfrac{1}{8}(1-\xi)(1-\eta)(1-\zeta) \\ N_2(\xi,\eta,\zeta) &= \tfrac{1}{8}(1+\xi)(1-\eta)(1-\zeta) \\ &\vdots \\ N_8(\xi,\eta,\zeta) &= \tfrac{1}{8}(1-\xi)(1+\eta)(1+\zeta) \end{aligned} \tag{8}$$

Edge Modes

There are $12(p-1)$ edge modes in the isotropic formulation. For example, the corresponding edge modes for edge 1 e.g. are:

$$^{E}N_i^{(1)}(\xi,\eta,\zeta) = \tfrac{1}{4}\phi_i(\xi)(1-\eta)(1-\zeta) \qquad i = 2,3,\ldots,p \tag{9}$$

where $\phi_i(\xi)$ is the function defined by (5).

Face Modes

There are $3(p-2)(p-3)$ face modes for $(p \geq 4)$. For example, the corresponding face modes for face 1 are:

$$^{F}N_{i,j}^{(1)}(\xi,\eta,\zeta) = \tfrac{1}{2}(1-\xi)\phi_i(\eta)\phi_j(\zeta) \tag{10}$$

where

$$i,j = 2,3,\ldots,p-2 \text{ and } i+j = 4,5,\ldots,p \tag{11}$$

Internal Modes

There are $(p-3)(p-4)(p-5)/6$ internal modes $(p \geq 6)$:

$$^{I}N_{i,j,k}^{(0)}(\xi,\eta,\zeta) = \phi_i(\xi)\phi_j(\eta)\phi_k(\zeta) \tag{12}$$

Anisotropic Space $\mathscr{S}^{p,p,q}$

1. *Nodal shape functions (Nodal modes)*
   There are eight nodal shape functions. These are the same as the shape functions used in the isotropic case, see formula (8).

2. *Edge Modes*
   There are $8(p-1)+4(q-1)$ edge modes. The modes for the edges 1-8 of degree 2, 3,..., *p,* which lie in the plane $\zeta = \pm 1$ are the same as in the isotropic case. The modes for the edges 9-12 of degree 2, 3,..., q lie in the planes $\xi = \pm 1$ and $\eta = \pm 1$. For example the modes of edge E_9:

$$ {}^{E}N_i^{(9)}(\xi,\eta,\zeta) = \tfrac{1}{4}\phi_i(\zeta)(1-\xi)(1-\eta) \qquad i = 2,3,...,q \tag{13} $$

3. *Face Modes*
   There are $4(p-1)(q-1)+(p-2)(p-3)$ face modes:

$$ \begin{aligned} &Face\ \xi = \pm 1: \\ &\left.\begin{aligned} {}^{F}N_{i,j}^{(1)}(\xi,\eta,\zeta) &= \tfrac{1}{2}(1-\xi)\phi_i(\eta)\phi_j(\zeta) \\ {}^{F}N_{i,j}^{(3)}(\xi,\eta,\zeta) &= \tfrac{1}{2}(1+\xi)\phi_i(\eta)\phi_j(\zeta) \end{aligned}\right\} \quad \begin{aligned} i &= 2,3,...,p \\ j &= 2,3,...,q \end{aligned} \\ &Face\ \eta = \pm 1: \\ &\left.\begin{aligned} {}^{F}N_{i,j}^{(2)}(\xi,\eta,\zeta) &= \tfrac{1}{2}(1-\eta)\phi_i(\xi)\phi_j(\zeta) \\ {}^{F}N_{i,j}^{(4)}(\xi,\eta,\zeta) &= \tfrac{1}{2}(1+\eta)\phi_i(\xi)\phi_j(\zeta) \end{aligned}\right\} \quad \begin{aligned} i &= 2,3,...,p \\ j &= 2,3,...,q \end{aligned} \\ &Face\ \zeta = \pm 1: \\ &\left.\begin{aligned} {}^{F}N_{i,j}^{(5)}(\xi,\eta,\zeta) &= \tfrac{1}{2}(1-\zeta)\phi_i(\xi)\phi_j(\eta) \\ {}^{F}N_{i,j}^{(6)}(\xi,\eta,\zeta) &= \tfrac{1}{2}(1+\zeta)\phi_i(\xi)\phi_j(\eta) \end{aligned}\right\} \quad \begin{aligned} i,j &= 2,3,...,p-2 \\ i+j &= 4,5,...,p \end{aligned} \end{aligned} \tag{14} $$

4. *Internal Modes*
   There are $(p-3)(p-2)(q-1)/2$ internal modes:

$$ {}^{I}N_{i,j,k}^{(0)}(\xi,\eta,\zeta) = \phi_i(\xi)\phi_j(\eta)\phi_k(\zeta) \tag{15} $$

where

$$ i,j = 2,3,...,p-2 \ \text{ and } \ i+j+k = 6,5,...,p \tag{16} $$

3 The blending function method

The computation of the full stress tensor by using the two-step-method requires higher order derivatives not only of the shape functions, but also of the mapping functions. Therefore the geometric shape of the newly developed 3D composite element is defined by a blending function method [8-10]. This method is mostly applied to *p*-version elements. Since in the *p*-version the size of the element is fixed, the representation of the curves and surfaces is very important. Detailed description of mapping by the blending function method is available in [6, 30]. The implementation of the blending function method in this investigation follows closely the work of Királyfalvi and Szabó [13].

4 Element equations

4.1 Displacement element formulation

The displacement $\mathbf{u}$ of the hierarchic 3D composite element is defined by nodal displacements $\mathbf{u}_i$ and the hierarchical displacement variables $\mathbf{a}_j$

$$\mathbf{u} = \mathbf{N}_i \mathbf{u}_i + \mathbf{N}_j \mathbf{a}_j = \hat{\mathbf{N}} \hat{\mathbf{u}} \,. \tag{17}$$

The matrix $\hat{\mathbf{N}}$ contains the nodal shape functions $\mathbf{N}_i \quad (i = 1,...,8)$ and the hierarchical shape functions $\mathbf{N}_j \quad (j = 9,...,\hat{n})$ and reads

$$\hat{\mathbf{N}} = \left[\underbrace{\mathbf{N}_1, \cdots, \mathbf{N}_8}_{\substack{\text{Nodal} \\ \text{Shape} \\ \text{Functions} \\ p=1}} \;\Big|\; \underbrace{f({}^E\mathbf{N}_p, {}^F\mathbf{N}_p, {}^I\mathbf{N}_p)}_{\substack{\text{Edge Modes} \\ \text{Face Modes} \\ \text{Internal Modes}}} \right], \tag{18}$$

where $\hat{n}$ represents the number of all hierarchical shape functions.

The element equations can be derived by using the principle of virtual work

$$\delta U_\varepsilon - \delta W = 0 \,. \tag{19}$$

The external virtual work is

$$\delta W = \delta \hat{\mathbf{u}}^T \mathbf{F}^i + \int_V \delta \mathbf{u}^T \mathbf{F}^B dV + \int_S \delta \mathbf{u}^T \mathbf{F}^S dS \tag{20}$$

where $\mathbf{F}^i$, $\mathbf{F}^B$ and $\mathbf{F}^S$ are the vectors of nodal forces, body forces and surface forces, respectively.

The internal virtual work is

$$\delta U_\varepsilon = \int_V \delta \boldsymbol{\varepsilon}^T \boldsymbol{\sigma} \, dV \,, \tag{21}$$

in which $\boldsymbol{\sigma}$ is the stress tensor.

The virtual displacements and strains are defined as follows

$$\delta \mathbf{u} = \hat{\mathbf{N}} \delta \hat{\mathbf{u}} \tag{22}$$

$$\delta \boldsymbol{\varepsilon} = \hat{\mathbf{B}} \delta \hat{\mathbf{u}} \,, \tag{23}$$

where $\hat{\mathbf{B}}$ represents the strain-displacement matrix

$$\hat{\mathbf{B}} = \begin{bmatrix} \frac{\partial N_1}{\partial x} & 0 & 0 & \frac{\partial N_{\hat{n}}}{\partial x} & 0 & 0 \\ 0 & \frac{\partial N_1}{\partial y} & 0 & 0 & \frac{\partial N_{\hat{n}}}{\partial y} & 0 \\ 0 & 0 & \frac{\partial N_1}{\partial z} & 0 & 0 & \frac{\partial N_{\hat{n}}}{\partial z} \\ \frac{\partial N_1}{\partial y} & \frac{\partial N_1}{\partial x} & 0 & \cdots \frac{\partial N_{\hat{n}}}{\partial y} & \frac{\partial N_{\hat{n}}}{\partial x} & 0 \\ \frac{\partial N_{i1}}{\partial z} & 0 & \frac{\partial N_1}{\partial x} & \frac{\partial N_{\hat{n}}}{\partial z} & 0 & \frac{\partial N_{\hat{n}}}{\partial x} \\ 0 & \frac{\partial N_1}{\partial z} & \frac{\partial N_1}{\partial y} & 0 & \frac{\partial N_{\hat{n}}}{\partial z} & \frac{\partial N_{\hat{n}}}{\partial y} \end{bmatrix}. \tag{24}$$

From equation (19) with substituting equations (22) and (23) the principle of virtual work becomes

$$\underbrace{\mathbf{F}^i + \int_V \hat{\mathbf{N}}^T \mathbf{F}^B dV + \int_S \hat{\mathbf{N}}^T \mathbf{F}^S dS}_{\mathbf{F}} = \underbrace{\int_V \hat{\mathbf{B}}^T \mathbf{C} \hat{\mathbf{B}}\, dV}_{\mathbf{K}}\, \hat{\mathbf{u}}\,. \tag{25}$$

4.2 The element stiffness matrix

The element stiffness matrix is given in [32]

$$\mathbf{K}^{(e)} = \int_{-1}^{1}\int_{-1}^{1}\int_{-1}^{1} \hat{\mathbf{B}}^T \mathbf{C}\, \hat{\mathbf{B}} \det \mathbf{J}\; d\xi d\eta d\zeta\,. \tag{26}$$

The stiffness matrix $\mathbf{C}$ with reference to the local element co-ordinate system is obtained from the stiffness matrix $\overline{\mathbf{C}}$ with reference to the fibre axis by using the coordinate transformation matrix $\mathbf{T}$

$$\mathbf{C} = \mathbf{T}\overline{\mathbf{C}}\mathbf{T}^T\,. \tag{27}$$

The integral is evaluated numerically by Gaussian quadrature. Usually, the stiffness matrix $\mathbf{C}$ is different from layer to layer and thus it is not a continuous function of ζ. Therefore the integration is carried out layerwise in order to obtain the stiffness coefficients for the entire element (see [20]). In order to apply the known coefficients of the Gaussian quadrature formula, the limits should be –1 and +1. This is achieved by suitably modifying the variable ζ to ζ_k in layer k such that ζ_k varies from –1 to +1 in that layer:

$$\zeta = -1 + \frac{1}{h}\left(-h_k(1-\zeta_k) + 2\sum_{j=1}^{k} h_j \right). \tag{28}$$

and

$$\frac{\partial \zeta}{\partial \zeta_k} = \frac{h_k}{h} \quad \rightarrow \quad \partial \zeta = \frac{h_k}{h} \partial \zeta_k \,. \tag{29}$$

Substitute (28) and (29) in (26), provides

$$\mathbf{K}^{(e)} = \sum_{k=1}^{n} \int_{-1}^{1} \int_{-1}^{1} \int_{-1}^{1} \hat{\mathbf{B}}^T \mathbf{C}^{(k)} \hat{\mathbf{B}} \frac{h_k}{h} \det \mathbf{J} \, d\xi d\eta d\zeta_k \,. \tag{30}$$

5 The two step method for analysis of composites

In the finite element method, the conventional displacement finite elements works fine with stress analysis of homogeneous materials. Even for computation of in-plane stresses in composite materials the displacement method provides excellent results. However, the results obtained for transverse stresses in laminated composite structures need an improvement due to the fact that there are discontinuities at layer interfaces. Therefore, the 3D composite element uses two steps to calculate the full stress tensor. In the first step the in-plane stresses are computed from the material law using a displacement approximation. In the second step the transverse stresses are calculated from the 3D equilibrium equations.

5.1 The in-plane stresses

The displacements are approximated using equation (17). Then, the strains become:

$$\boldsymbol{\varepsilon} = \mathbf{D}\mathbf{u} = \mathbf{D}\hat{\mathbf{N}}\hat{\mathbf{u}} = \hat{\mathbf{B}}\hat{\mathbf{u}} \,. \tag{31}$$

By means of the constitutive law the stresses are obtained as:

$$\boldsymbol{\sigma}^{(k)} = \mathbf{C}^{(k)}\boldsymbol{\varepsilon} = \mathbf{C}^{(k)}\hat{\mathbf{B}}\hat{\mathbf{u}} \tag{32}$$

In the development of the finite 3D composite element, it is necessary to identify globally (G) and locally (L) continuous variables. Following the definition of Hoa and Feng [11] the stresses $\boldsymbol{\sigma}$ and strains $\boldsymbol{\varepsilon}$ can be divided into in-plane and transverse parts:

$$\boldsymbol{\sigma}_L^{(k)} = \begin{pmatrix} \sigma_x \\ \sigma_y \\ \tau_{xy} \end{pmatrix}^{(k)} \qquad \boldsymbol{\varepsilon}_G = \begin{pmatrix} \varepsilon_x \\ \varepsilon_y \\ \gamma_{xy} \end{pmatrix}$$
$$\text{and} \tag{33}$$
$$\boldsymbol{\sigma}_G^{(k)} = \begin{pmatrix} \sigma_z \\ \tau_{xz} \\ \tau_{yz} \end{pmatrix}^{(k)} \qquad \boldsymbol{\varepsilon}_L = \begin{pmatrix} \varepsilon_z \\ \gamma_{xz} \\ \gamma_{yz} \end{pmatrix}$$

Hence, globally variables are those that are continuous across the thickness of the laminate and therefore continuous at the layer interfaces. Locally variables are those that are continuous only across the thickness of each layer but not necessarily continuous at the layer interfaces.

Correspondingly, the constitutive equation can be expressed in the form

$$\begin{pmatrix} \boldsymbol{\sigma}_L \\ \boldsymbol{\sigma}_G \end{pmatrix}^{(k)} = \begin{bmatrix} \mathbf{C}_1 & \mathbf{C}_2 \\ \mathbf{C}_2^T & \mathbf{C}_3 \end{bmatrix}^{(k)} \begin{pmatrix} \boldsymbol{\varepsilon}_G \\ \boldsymbol{\varepsilon}_L \end{pmatrix}. \tag{34}$$

The in-plane stresses become

$$\boldsymbol{\sigma}_L^{(k)} = \begin{bmatrix} \mathbf{C}_1 & \mathbf{C}_2 \end{bmatrix}^{(k)} = \mathbf{C}_L^{(k)} \hat{\mathbf{B}} \hat{\mathbf{u}}. \tag{35}$$

5.2 The transverse stresses

The second step involves calculation of the out-of-plane stresses from the equilibrium equations using the in-plane stresses calculated in the first step.

The equilibrium equations for the *k*-th layer have the form:

$$\begin{aligned} \frac{\partial \sigma_x^{(k)}}{\partial x} + \frac{\partial \tau_{xy}^{(k)}}{\partial y} + \frac{\partial \tau_{xz}^{(k)}}{\partial z} &= 0, \\ \frac{\partial \tau_{xy}^{(k)}}{\partial x} + \frac{\partial \sigma_y^{(k)}}{\partial y} + \frac{\partial \tau_{yz}^{(k)}}{\partial z} &= 0, \\ \frac{\partial \tau_{xz}^{(k)}}{\partial x} + \frac{\partial \tau_{yz}^{(k)}}{\partial y} + \frac{\partial \sigma_z^{(k)}}{\partial z} &= 0. \end{aligned} \tag{36}$$

Resolving for transverse stresses and integrating equation (36) leads to:

$$\begin{aligned} \tau_{xz}^{(k)} &= -\int_z \frac{\partial \sigma_x^{(k)}}{\partial x} + \frac{\partial \tau_{xy}^{(k)}}{\partial y} \, dz + \psi_{xz}^{(k)}(x, y) \\ \tau_{yz}^{(k)} &= -\int_z \frac{\partial \tau_{xy}^{(k)}}{\partial x} + \frac{\partial \sigma_y^{(k)}}{\partial y} \, dz + \psi_{yz}^{(k)}(x, y) \\ \sigma_z^{(k)} &= -\int_z \frac{\partial \tau_{xz}^{(k)}}{\partial x} + \frac{\partial \tau_{yz}^{(k)}}{\partial y} \, dz + \psi_z^{(k)}(x, y) \end{aligned} \tag{37}$$

By satisfying the boundary conditions at the top und bottom surfaces the unknown functions $\psi_{xz}^{(1)}$ and $\psi_{xz}^{(N)}$ can be computed. The remaining functions $\psi_{xz}^{(2)}, \ldots, \psi_{xz}^{(N-1)}$ are computed using the interface conditions. The same applies to the functions $\psi_{yz}^{(k)}$ and $\psi_z^{(k)}$. It has to be pointed out, that there are in total 3(*N*+1) internal and external conditions to compute 3*N* unknown functions. Therefore, only 3*N* conditions can be satisfied. One of the boundary conditions for each transverse stress component remains unsatisfied. However, if the 3D solution obtained for the displacements converges to the exact one the remaining discontinuities of all three transverse stress components at one of the surfaces must converge to zero. Hence, when increasing the polynomial order the remaining discontinuity of each of the transverse stress components should vanish [5].

5.2.1 The transverse shear stresses

The transverse shear stresses read

$$\boldsymbol{\tau}_G^{(k)} = \begin{pmatrix} \tau_{xz} \\ \tau_{yz} \end{pmatrix}^{(k)} = -\int_z \left(\mathbf{A}_x \boldsymbol{\sigma}_{L,x}^{(k)} + \mathbf{A}_y \boldsymbol{\sigma}_{L,y}^{(k)} \right) dz + \boldsymbol{\psi}_\tau^{(k)} \tag{38}$$

with $\mathbf{A}_x$ and $\mathbf{A}_y$ denoting Boolean matrices of the form:

$$\mathbf{A}_x = \begin{bmatrix} 1 & 0 & 0 \\ 0 & 0 & 1 \end{bmatrix} \text{ and } \mathbf{A}_y = \begin{bmatrix} 0 & 0 & 1 \\ 0 & 1 & 0 \end{bmatrix}. \tag{39}$$

The first derivatives of the in-plane stresses (35) are:

$$\boldsymbol{\sigma}_{L,x}^{(k)} = \mathbf{C}_L^{(k)} \hat{\mathbf{B}}_{,x} \hat{\mathbf{u}} \,, \tag{40}$$

$$\boldsymbol{\sigma}_{L,y}^{(k)} = \mathbf{C}_L^{(k)} \hat{\mathbf{B}}_{,y} \hat{\mathbf{u}} \,. \tag{41}$$

Substituting equation (40) and (41) in (38) provides:

$$\boldsymbol{\tau}_G^{(k)} = \begin{pmatrix} \tau_{xz} \\ \tau_{yz} \end{pmatrix}^{(k)} = -\int_z \left(\mathbf{A}_x \mathbf{C}_L^{(k)} \hat{\mathbf{B}}_{,x} \hat{\mathbf{u}} + \mathbf{A}_y \mathbf{C}_L^{(k)} \hat{\mathbf{B}}_{,y} \hat{\mathbf{u}} \right) dz + \boldsymbol{\psi}_\tau^{(k)} \,. \tag{42}$$

Equation (42) is modified by introducing the normalized co-ordinate ζ as follows

$$z = \frac{h}{2} \zeta \tag{43}$$

and hence

$$\boldsymbol{\tau}_G^{(k)} = \begin{pmatrix} \tau_{xz} \\ \tau_{yz} \end{pmatrix}^{(k)} = -\frac{h}{2} \left\{ \mathbf{A}_x \mathbf{C}_L^{(k)} \int_\zeta \hat{\mathbf{B}}_{,x} d\zeta + \mathbf{A}_y \mathbf{C}_L^{(k)} \int_\zeta \hat{\mathbf{B}}_{,y} d\zeta \right\} \hat{\mathbf{u}} + \boldsymbol{\psi}_\tau^{(k)} \tag{44}$$

5.2.2 The transverse normal stress

The transverse normal stress in (37) can be written as

$$\begin{aligned} \sigma_z^{(k)} &= -\int_z \frac{\partial \tau_{xz}^{(k)}}{\partial x} + \frac{\partial \tau_{yz}^{(k)}}{\partial y} dz + \psi_z^{(k)}(x, y) \\ \sigma_z^{(k)} &= \int_z \left\{ \int_z \frac{\partial^2 \sigma_x^{(k)}}{\partial x^2} + \frac{\partial^2 \sigma_y^{(k)}}{\partial y^2} + 2 \frac{\partial^2 \tau_{xy}^{(k)}}{\partial x \partial y} dz + \psi_{xz,x}^{(k)}(x, y) + \psi_{yz,y}^{(k)}(x, y) \right\} dz + \psi_z^{(k)}(x, y). \end{aligned} \tag{45}$$

The second derivatives of the in-plane stresses (35) are

$$
\begin{aligned}
\boldsymbol{\sigma}_{L,xx}^{(k)} &= \mathbf{C}_L^{(k)} \hat{\mathbf{B}}_{,xx} \hat{\mathbf{u}} \\
\boldsymbol{\sigma}_{L,yy}^{(k)} &= \mathbf{C}_L^{(k)} \hat{\mathbf{B}}_{,yy} \hat{\mathbf{u}} \\
\boldsymbol{\sigma}_{L,xy}^{(k)} &= \mathbf{C}_L^{(k)} \hat{\mathbf{B}}_{,xy} \hat{\mathbf{u}}
\end{aligned}
\tag{46}
$$

Using equation (46) with (45) leads to

$$
\begin{aligned}
\sigma_z^{(k)} = \int_z \Bigg\{ \int_z \Big(\mathbf{e}_1^T \mathbf{C}_L^{(k)} \hat{\mathbf{B}}_{,xx} + \mathbf{e}_2^T \mathbf{C}_L^{(k)} \hat{\mathbf{B}}_{,yy} + 2\mathbf{e}_3^T \mathbf{C}_L^{(k)} \hat{\mathbf{B}}_{,xy} \Big) dz\, \hat{\mathbf{u}} + \\
\psi_{xz,x}^{(k)}(x,y) + \psi_{yz,y}^{(k)}(x,y)\, dz \Bigg\} + \psi_z^{(k)}(x,y)
\end{aligned}
\tag{47}
$$

with

$$
\mathbf{e}_1^T = \{1 \quad 0 \quad 0\}; \quad \mathbf{e}_2^T = \{0 \quad 1 \quad 0\}; \quad \mathbf{e}_3^T = \{0 \quad 0 \quad 1\}. \tag{48}
$$

By using the normalized co-ordinate ζ given in equation (43) the transverse normal stress can be expressed as

$$
\begin{aligned}
\sigma_z^{(k)} = \frac{h^2}{4} \Bigg\{ \mathbf{e}_1^T \mathbf{C}_L^{(k)} \int_\zeta \int_\zeta \hat{\mathbf{B}}_{,xx} d\zeta d\zeta + \mathbf{e}_2^T \mathbf{C}_L^{(k)} \int_\zeta \int_\zeta \hat{\mathbf{B}}_{,yy} d\zeta d\zeta + 2\mathbf{e}_3^T \mathbf{C}_L^{(k)} \int_\zeta \int_\zeta \hat{\mathbf{B}}_{,xy} d\zeta d\zeta \Bigg\} \hat{\mathbf{u}} \\
+ \frac{h}{2} \int_\zeta \Big(\psi_{xz,x}^{(k)}(x,y) + \psi_{yz,y}^{(k)}(x,y) \Big) d\zeta + \psi_z^{(k)}(x,y).
\end{aligned}
\tag{49}
$$

6 Numerical examples

The finite element program B2000 was used for testing the presented element. Simply supported layered composite plates under sinusoidal load were considered a suitable test case since significant transverse stresses occur and for rectangular layered composite an analytical 3D elasticity solution is also available. The plate is shown in Figure 4.

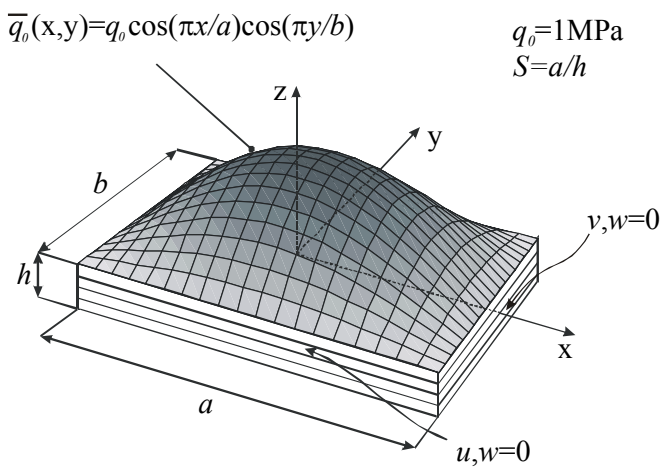

Figure 4: Simply supported laminated plate

The edge lengths in x- and y-direction are a and b, respectively. The plate thickness is h. A fibre orientation of zero indicates that the longitudinal direction of the fibres is parallel to the x-axis. The stresses presented are normalized by pressure amplitude q_0 and slenderness S:

$$
\begin{aligned}
&(\bar{\sigma}_x, \bar{\sigma}_y) = \frac{1}{q_0 S^2}(\sigma_x, \sigma_y) \\
&(\bar{\tau}_{xz}, \bar{\tau}_{yz}) = \frac{1}{q_0 S}(\tau_{xz}, \tau_{yz}) \\
&S = \frac{a}{h}, \quad \bar{z} = \frac{z}{h}
\end{aligned}
\tag{50}
$$

The locations for values of stresses for the analytical solutions are:

$$
\begin{aligned}
&\sigma_x, \sigma_y, \sigma_z : \quad (0, 0, z) \\
&\tau_{xz} : \quad (-0.5a, 0, z) \\
&\tau_{yz} : \quad (0, -0.5b, z)
\end{aligned}
\tag{51}
$$

Whereas the values of stresses for numerical theories are the nearest optimal points refer to (51). The various examples considered are as follows:

EXAMPLE 1: A simply supported square (a/b=1) laminated cross-ply pate with a stacking sequence of [0/90/90/0] and four equal ply thicknesses is considered to validate the present theory through comparison with three-dimensional elasticity solution and a closed-form solution of a higher-order plate theory. The material properties considered for this example are:

$$
\begin{aligned}
&\frac{E_1}{E_2} = \frac{E_1}{E_3} = 25, \quad \frac{G_{12}}{E_2} = \frac{G_{13}}{E_3} = 0.5, \quad \frac{G_{22}}{E_3} = 0.2 \\
&\nu_{12} = \nu_{23} = \nu_{13} = 0.25
\end{aligned}
\tag{52}
$$

The calculations were carried out using a finite element mesh of 5×5×2 elements. The variation of in-plane normal stress $\bar{\sigma}_x$ in fibre direction with the plate slenderness $S=a/h$ for the present theory is presented in Figure 5. This comparative study shows the accuracy also for thin plate bending and proves that in cases of thin structures no shear locking occurs. In Figure 6 the in-plane stress distribution of the present element for a plate with S=4 is compared with 3D elasticity [18], closed form solution of a higher order laminatewise plate theory [21] and the first order shear deformation theory [32]. This example indicates that the FSDT is not able to obtain accurate stresses for moderately thick plates. Also the higher order plate theory does not predict the stress value at the internal interface accurately. The transverse shear stresses are presented in Figure 7 and Figure 8. In addition to the 3D elasticity here a comparison is also made with stresses obtained by the extended 2D-method [27, 28] as implemented into TRAVEST.

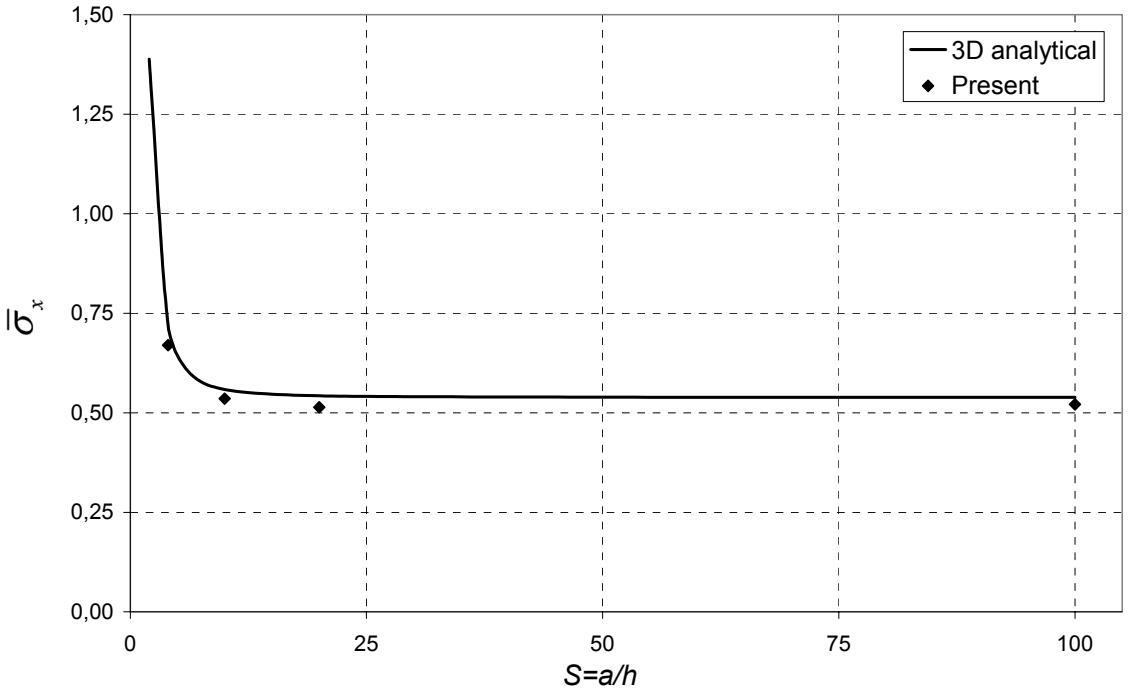

Figure 5: Effect of plate slenderness S=a/h on the in-plane normal stress for a four equal layer cross-ply[0,90,90,0] plate

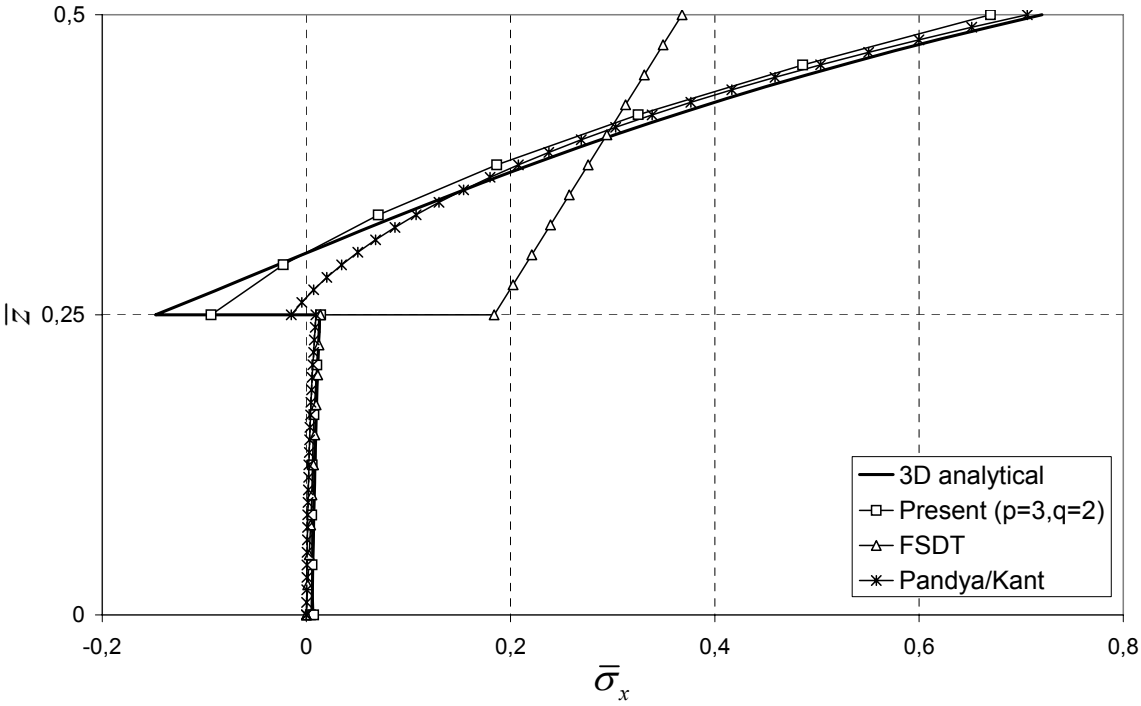

Figure 6: Comparison of in-plane stresses $\bar{\sigma}_x$ for a four equal layer cross-ply [0,90,90,0] plate with S=4

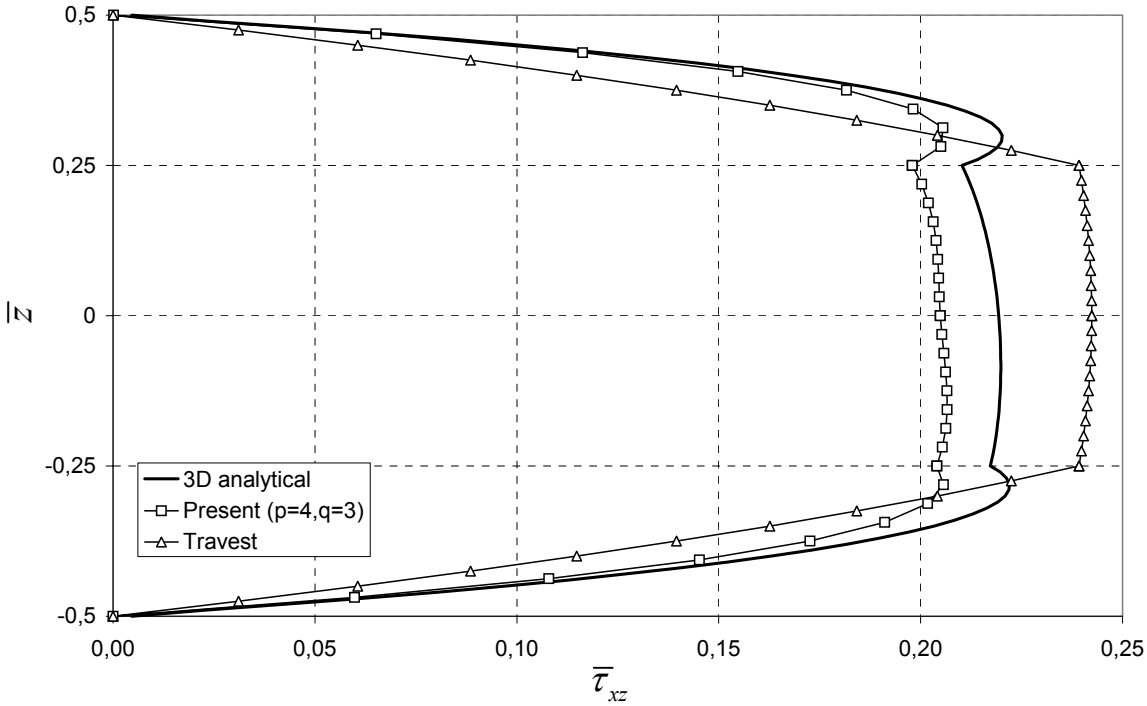

Figure 7: Comparison of transverse shear stress $\overline{\tau}_{xz}$ for a four equal layer cross-ply [0,90,90,0] plate with S=4

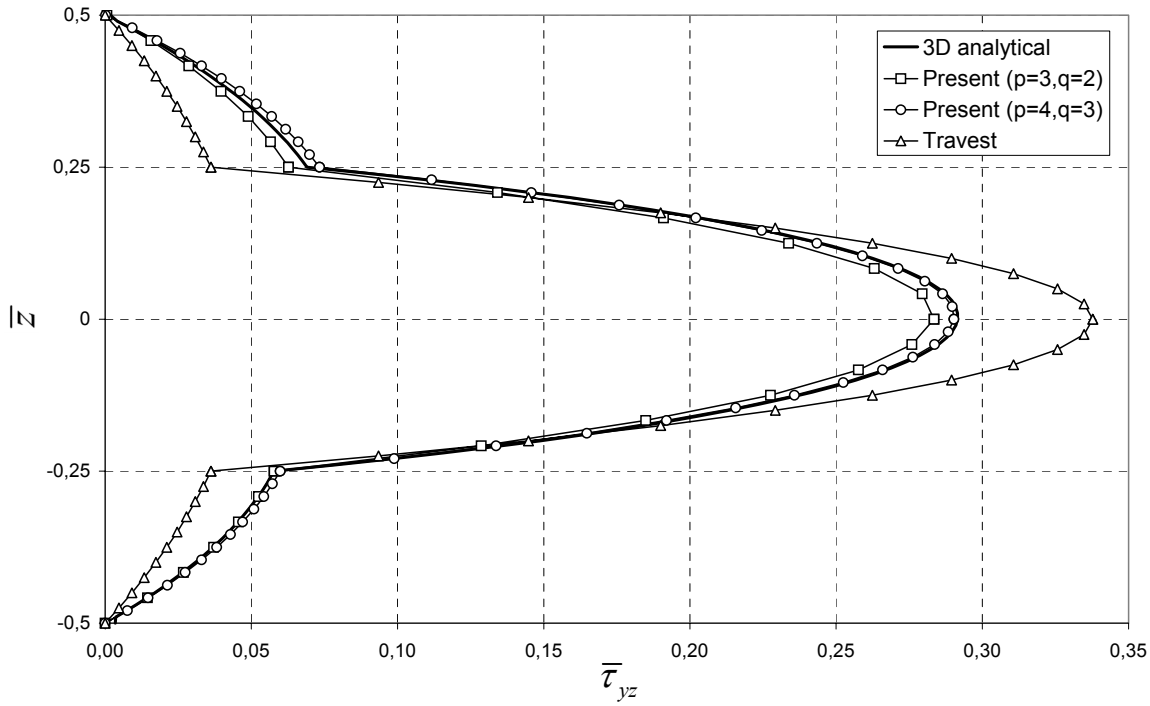

Figure 8: Comparison of transverse shear stress $\overline{\tau}_{yz}$ for a four equal layer cross-ply[0,90,90,0] plate with S=4

EXAMPLE 2: In this example a rectangular (a/b = 1.48341, $S = a/h$ = 5) plate with a stacking sequence of [0/90/90/0] and four equal ply thicknesses are considered. For this case calculations were carried out using a finite element mesh of 7×5×1 elements. The material properties considered for this example are:

$$
\begin{aligned}
E_L &= 138000 \text{ MPa} \\
E_T &= 9300 \text{ MPa} \\
\nu_{LT} &= 0.3 \\
\nu_{TT} &= 0.48 \\
G_{LT} &= 4600 \text{ MPa} \\
G_{TT} &= 3100 \text{ MPa.}
\end{aligned}
$$

Figure 9 depicts distributions of the in-plane stresses σ_x and σ_y over the plate thickness at the centre of the plate. The presented two step method is compared to an analytical elasticity solution. In addition, the solution of a 20-noded composite brick element (MSC.MARC 3D), which uses the material to obtain the full stress tensor, is shown. The results received by the two step method as well as by the MSC.MARC 3D composite element are close to the analytical solution. The result indicates that a small *p*-order of two or three within the two step method is sufficient for calculating the in-plane stresses. This holds for the transverse stresses, too. The results are displayed in Figure 10.

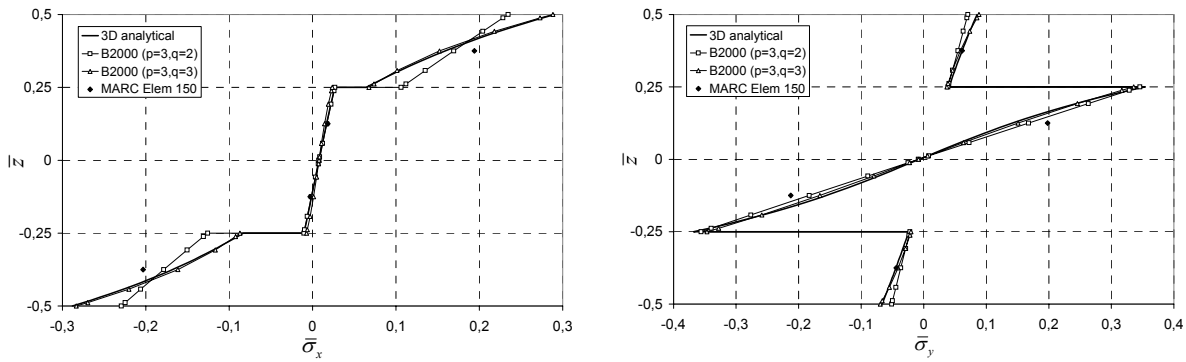

Figure 9:Comparison of in-plane stresses $\bar{\sigma}_x$ and $\bar{\sigma}_y$ for a four equal layer cross-ply [0,90,90,0] plate with S=5

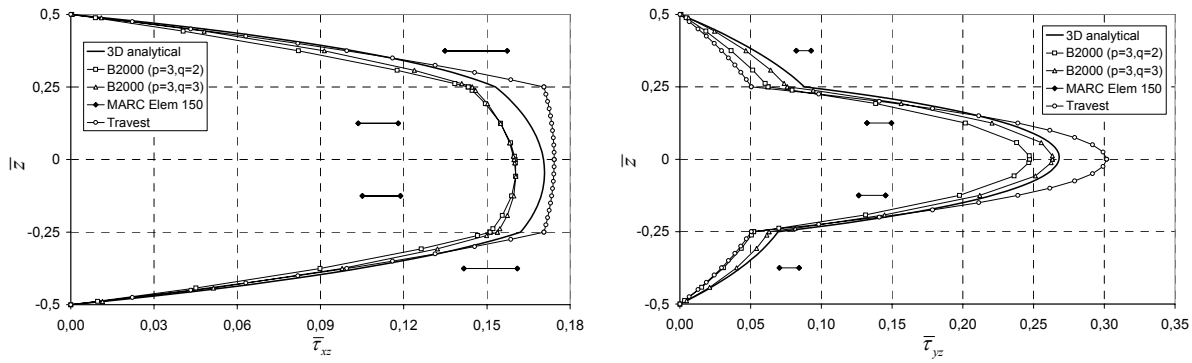

Figure 10: Comparison of transverse shear stresses $\bar{\tau}_{xz}$ and $\bar{\tau}_{yz}$ for a four equal layer cross-ply [0,90,90,0] plate with S=5

In Figure 11 the transverse normal stress is displayed. The solution of the new hierarchical composite elements is close to the exact one. The MSC.MARC composite elements show a satisfactory approximation of this stress component. However, none of the results provided by the MSC.MARC 3D composite brick element shows reliable transverse stresses τ_{xz} and τ_{yz}. The distribution of the transverse stress component τ_{xz} is in sharp contrast to the distribution

of the 3D solutions. The distribution of τ_{yz} is comparable to the corresponding three dimensional solution, however the difference in accuracy is significant.

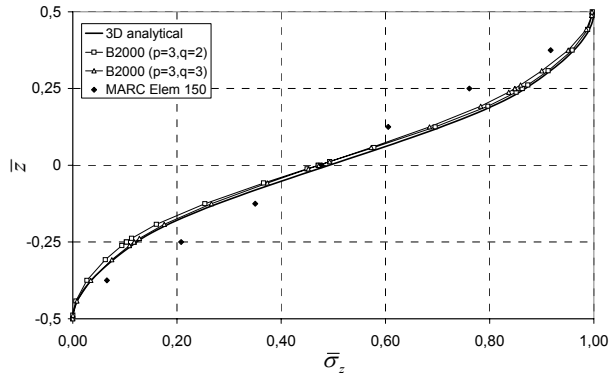

Figure 11: Comparison of transverse normal stress $\bar{\sigma}_z$ for a four equal layer cross-ply [0,90,90,0] plate with S=5

EXAMPLE 3: In this example a square plate (and *a/b*=1 and *S* = 4) with a stacking sequence of $[(+45/90/-45/0)_2]_S$ and ply thicknesses of [0.0625] is considered. The solutions were carried out using 7×7×4 elements. The results of the in-plane and transverse stresses are shown in Figure 12 to Figure 14. The two step method compares very well with the costly 3D-FEM solution obtained by means of HEX8 elements of MSC.NASTRAN (three elements per layer in thickness direction).

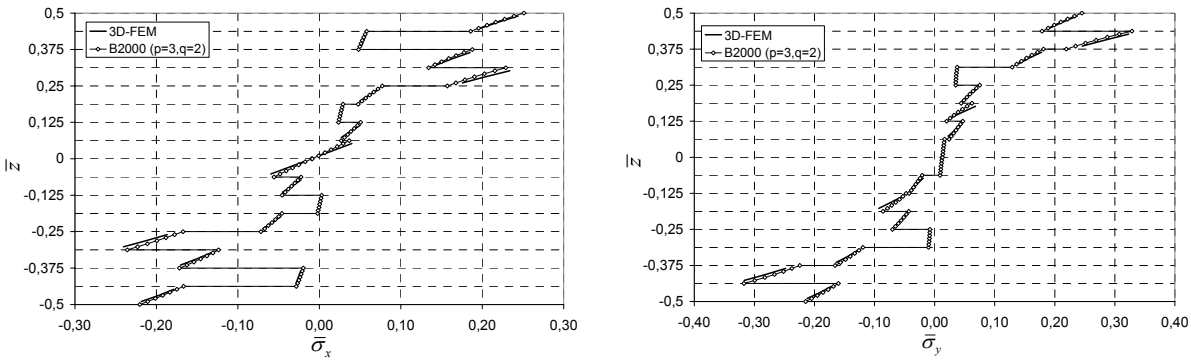

Figure 12: Comparison of in-plane stresses $\bar{\sigma}_x$ and $\bar{\sigma}_y$

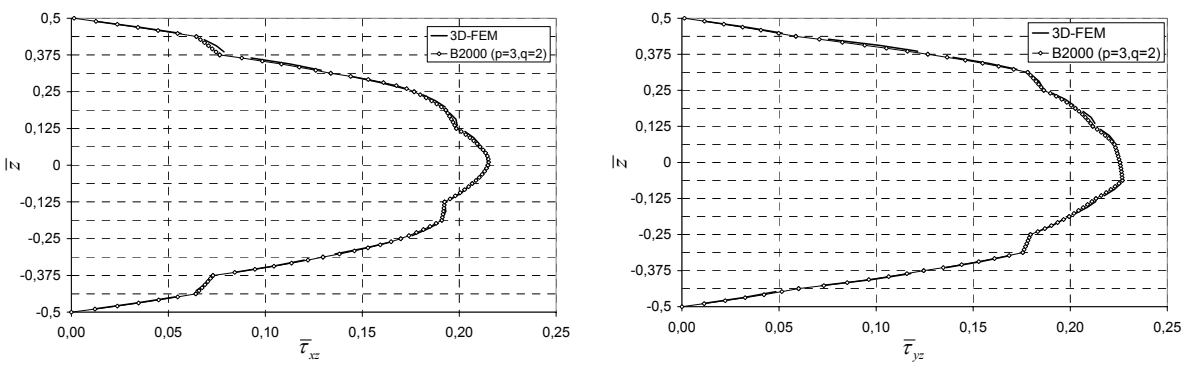

Figure 13: Comparison of transverse shear stresses $\bar{\tau}_{xz}$ and $\bar{\tau}_{yz}$

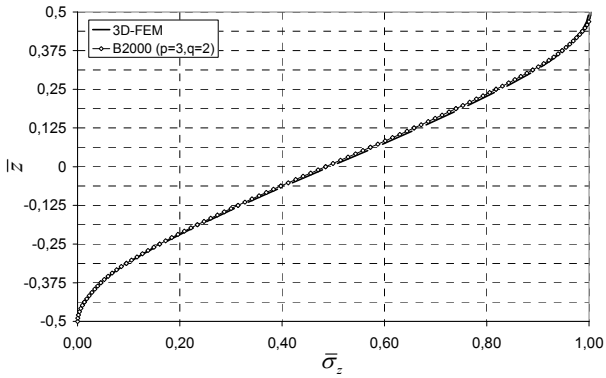

Figure 14: Comparison of transverse normal stress $\bar{\sigma}_z$

These examples indicate that it is difficult to calculate transverse shear stresses with high accuracy using only the material law and a displacement field, which is interpolated by quadratic isoparametric shape functions. Since the in-plane displacements of thick structures show pronounced zig-zag distributions in thickness direction the calculated transverse stresses are not useable as shown in example 2 (MARC solution). The two step method uses the displacement field and the material law only for calculating the in-plane stresses, whereas the transverse stresses are calculated from 3D equilibrium conditions. Highly accurate results for the out-of-plane stresses are obtained in a very efficient way, since layerwise discretization in thickness direction can be avoided.

7 Conclusion

A 3D finite element for calculating the full stress tensor in composite structures has been developed. Based on 3D linear elasticity theory and using the material law as well as the 3D equilibrium equations excellent results are achieved. In contrasted to shell elements, which are used by postprocessor tools like TRAVEST for improving out-of-plane stresses, the present elements can be used for efficiently analysing thick composite structures.

References

[1] Actis, R. L.; Szabó, B. A.; Schwab, C.: *Hierarchic models for laminated plates and shells*. Computer Methods in Applied Mechanics and Engineering *172,* 79-107 (1999).

[2] Babuška, I.; Szabó, B. A.; Actis, R. L.: *Hierarchic models for laminated composites*. International Journal for Numerical Methods in Engineering *33,* 503-535 (1992).

[3] Babuška, I.; Szabó, B. A.; Katz, I. N.: *The p-version of the finite element method*. SIAM journal on numerical analysis *18,* 515-545 (1981).

[4] Barker, R. M.; Lin, F.-T.; Dana, J. R.: *Three-dimensional finite element analysis of laminated composites*. Computers & Structures *2,* 1013-1029 (1972).

[5] Bogdanovich, A. E.; Pastore, C. M.; Deepak, B. P.: *A comparison of various 3-D approaches for the analysis of laminated composite structures*. Composites Engineering *5,* 1105-1126 (1995).

[6] Düster, A.; Bröker, H.; Rank, E.: *The p-version of the finite element method for three-dimensional curved thin walled structures*. International Journal for Numerical Methods in Engineering *52,* 673-703 (2001).

[7] Düster, A.; Rank, E.: *The p-version of the finite element method compared to an adaptive h-version for the deformation theory of plasticity*. Computer Methods in Applied Mechanics and Engineering *190,* 1925-1935 (2001).

[8] Gordon, W. J.: *Blending-function methods of bivariate and multivariate interpolation and approximation*. SIAM journal on numerical analysis *8,* 158-177 (1971).

[9] Gordon, W. J.; Hall, C. A.: *Construction of curvilinear co-ordinate systems and applications to mesh generation*. International Journal for Numerical Methods in Engineering *7,* 461-477 (1973).

[10] Gordon, W. J.; Hall, C. A.: *Transfinite element methods: blending-function interpolation over arbitrary curved element domains*. Numer Mathe *21,* 109-129 (1973).

[11] Hoa, S. V.; Feng, W.: Hybrid finite element method for stress analysis of laminated composites, Kluwer Academic Publishers, Boston/Dordrecht/London 1998.

[12] Hoa, S. V.; Yu, C. W.; Sankar, T. S.: *Analysis of Filament Wound Vessel Using Finite Elements*. Composite Structures *3,* 1-18 (1985).

[13] Királyfalvi, G.; Szabó, B. A.: *Quasi-regional mapping for the p-version of the finite element method*. Finite Elements in Analysis and Design *27,* 85-97 (1997).

[14] Kirchhoff, G. R.: *Über das Gleichgewicht und die Bewegung einer elastischen Scheibe*. Journal für reine und angewandte Mathematik *40,* 51-88 (1850).

[15] Mindlin, R. D.: *Influence of Rotatory Inertia and Shear on Flexural Motions of Isotropic, Elastic Plates*. Journal of Applied Mechanics *18,* 31-38 (1951).

[16] Natarajan, R.; Hoa, S. V.; Sankar, T. S.: *Stress analysis of filament wound tanks using three-dimensional finite elements*. International Journal for Numerical Methods in Engineering *23,* 623-633 (1986).

[17] Noor, A. K.; Burton, W. S.: *Assessment of shear theories for multilayered composite plates*. Appl Mech Rev *42,* 1-13 (1989).

[18] Pagano, J. N.: *Exact solutions for rectangular bidirectional composites and sandwich plates*. Journal of Composite Materials *4,* 20-35 (1970).

[19] Pagano, N. J.; Hatfield, S. J.: *Elastic Behavior of Multilayered Bidirectional Composites*. AIAA Journal *10,* 931-933 (1972).

[20] Panda, S.; Natarajan, R.: *Finite element anaylsis of laminated composite plates*. International Journal for Numerical Methods in Engineering *14,* 69-79 (1979).

[21] Pandya, B. N.; Kant, T.: *Flexural Analysis of Laminated Composites Using Refined Higher-Order C^0 Plate Bending Elements.* Computer Methods in Applied Mechanics and Engineering *66,* 173-198 (1988).

[22] Pryor, C. W.; Barker, R. M.: *A finite-element analysis including transverse shear effects for applications to laminated plates*. AIAA *9,* 912-917 (1971).

[23] Reddy, J. N.: *A review of refined theories of laminated composite plates*. Shock and vibration digest *22,* 3-17 (1990).

[24] Reissner, E.: *The Effect of transverse shear deformation on the bending of elastic plates*. Journal of Applied Mechanics *12,* 69-77 (1945).

[25] Rohwer, K.: Improved Transverse Shear Stiffnesses for Layered Finite Elements. Forschungsbericht DFVLR-FB 88-32. (1988)

[26] Rohwer, K.: *Application of Higher-Order Theories to the Bending Analysis of Layered Composite Plates*. International Journal of Solids and Structures *29,* 105-119 (1992).

[27] Rolfes, R.; Rohwer, R.: *Improved Transverse Shear Stresses in Composite Finite Elements Based on First Order Shear Deformation Theory*. Int J Num Meth *40,* 51-60 (1997).

[28] Rolfes, R.; Rohwer, R.; Ballerstaedt, M.: *Efficient Linear Transverse Normal Stress Analysis of Layered Composite Plates*. Computers and Structures *68,* 643-652 (1998).

[29] Szabó, B. A.: *Implementation of a finite element software system with h and p extension capabilties*. Finite Elements in Analysis and Design *2,* 177-194 (1986).

[30] Szabó, B. A.; Babuška, I.: Finite Element analysis, John Wiley & Sons, Inc., New York 1991.

[31] Szabó, B. A.; Sahrmann, G. J.: *Hierarchic plate and shell models based on p-extension*. International Journal for Numerical Methods in Engineering *26,* 1855-1881 (1988).

[32] Whitney, J. M.; Pagano, N. J.: *Shear Deformation in Heterogeneous Anisotropic Plates*. Journal of Applied Mechanics *37,* 1031-1036 (1970).

[33] Zienkiewicz, O. C.; Gago, J. P. d. S. R.; Kelly, D. W.: *The hierarchical concept in finite element analysis*. Computers & Structures *16,* 53-65 (1983).

[34] Zienkiewicz, O. C.; Taylor, R. L.: The Finite Element Method, Butterworth-Heinemann, Oxford 2000.